Bioorganic & Medicinal Chemistry xxx (2012) xxx–xxx

Contents lists available at SciVerse ScienceDirect

Bioorganic & Medicinal Chemistry

journal homepage: www.elsevier.com/locate/bmc

N^4-Phenyl-substituted 2-acetylpyridine thiosemicarbazones: Cytotoxicity against human tumor cells, structure–activity relationship studies and investigation on the mechanism of action

Marcella A. Soares [a,b], Josane A. Lessa [c], Isolda C. Mendes [d], Jeferson G. Da Silva [c], Raquel G. dos Santos [b,e], Lívia B. Salum [f], Hikmat Daghestani [g], Adriano D. Andricopulo [f], Billy W. Day [h], Andreas Vogt [i], Jorge L. Pesquero [a], Willian R. Rocha [c], Heloisa Beraldo [c,*]

[a] Departamento de Fisiologia e Biofísica, Universidade Federal de Minas Gerais, 31270-901 Belo Horizonte, MG, Brazil
[b] Centro de Desenvolvimento de Tecnologia Nuclear, CDTN, 31270-901 Belo Horizonte, MG, Brazil
[c] Departamento de Química, Universidade Federal de Minas Gerais, 31270-901 Belo Horizonte, MG, Brazil
[d] Escola de Belas Artes, Departamento de Artes Plásticas, Universidade Federal de Minas Gerais, 31270-901 Belo Horizonte, MG, Brazil
[e] Instituto Nacional de Ciência e Tecnologia de Medicina Molecular, Faculdade de Medicina, Universidade Federal de Minas Gerais, 30130-100 Belo Horizonte, MG, Brazil
[f] Centro de Biotecnologia Molecular Estrutural, Instituto de Física de São Carlos, Universidade de São Paulo, 13560-970 São Carlos, SP, Brazil
[g] Department of Structural Biology, University of Pittsburgh, Pittsburgh, PA 15260, USA
[h] Department of Pharmaceutical Sciences, University of Pittsburgh, Pittsburgh, PA 15261, USA
[i] University of Pittsburgh Drug Discovery Institute, University of Pittsburgh, Pittsburgh, PA 15261, USA

ARTICLE INFO

Article history:
Received 9 March 2012
Revised 5 April 2012
Accepted 10 April 2012
Available online xxxx

Keywords:
2-Acetylpyridine thiosemicarbazones
Glioblastoma
Breast cancer
Cytotoxicity
Tubulin

ABSTRACT

N^4-Phenyl 2-acetylpyridine thiosemicarbazone (H2Ac4Ph; *N*-(phenyl)-2-(1-(pyridin-2-yl)ethylidene) hydrazinecarbothioamide) and its N^4-*ortho*-, -*meta*- and -*para*-fluorophenyl (H2Ac4*o*FPh, H2Ac4*m*FPh, H2Ac4*p*FPh), N^4-*ortho*-, -*meta*- and -*para*-chlorophenyl (H2Ac4*o*ClPh, H2Ac4*m*ClPh, H2Ac4*p*ClPh), N^4-*ortho*-, -*meta*- and -*para*-iodophenyl (H2Ac4*o*IPh, H2Ac4*m*IPh, H2Ac4*p*IPh) and N^4-*ortho*-, -*meta*- and -*para*-nitrophenyl (H2Ac4*o*NO_2Ph, H2Ac4*m*NO_2Ph, H2Ac4*p*NO_2Ph) derivatives were assayed for their cytotoxicity against human malignant breast (MCF-7) and glioma (T98G and U87) cells. The compounds were highly cytotoxic against the three cell lineages (IC_{50}: MCF-7, 52–0.16 nM; T98G, 140–1.0 nM; U87, 160–1.4 nM). All tested thiosemicarbazones were more cytotoxic than etoposide and did not present any haemolytic activity at up to 10^{-5} M. The compounds were able to induce programmed cell death. H2Ac4*p*ClPh partially inhibited tubulin assembly at high concentrations and induced cellular microtubule disorganization.

1. Introduction

In 2030 an estimated 12 million deaths from cancer are projected in the world.[1] Breast cancer, one of the highest incident types, affects more than one million women every year.[2] Treatment options for patients with advanced breast cancer are varied and include endocrine therapies, chemotherapies and targeted therapies. Nonetheless, the high mortality evoked by this pathology is related to the resistance of breast tumor cells to conventional therapy.[3]

Malignant gliomas are the most frequent and lethal cancers originating in the central nervous system and the second most common form of cancer in pediatric patients.[4] Malignant gliomas are classified as astrocytomas, oligodendrogliomas, and oligoastrocytomas and are histologically graded as II, III, or IV by WHO. The most aggressive, grade IV, astrocytoma is referred to as glioblastoma multiforme.[5] Traditionally, patients with glioblastoma multiforme have been managed with surgery followed by radiotherapy. More recently, the oral alkylating agent temozolamide has become the standard of care for the management of glioblastoma multiforme.[6] Other alternative chemotherapy agents, such as etoposide, carboplatin and nitrosurea-containing procarbazine, lomustine and vincristine, have also been studied.[7] These therapies produce, however, only a short median survival time.[8] Moreover, the low tolerance of the central nervous system to conventional chemotherapeutic agents impairs the effectiveness of the treatment.[9] Thus, it is important to search for novel drug candidates in order to overcome these challenges.

Thiosemicarbazones constitute an interesting class of compounds with a wide spectrum of pharmacological applications.[10] α(N)-Heterocyclic thiosemicarbazones have been extensively investigated as potential anticancer agents.[11] The search for an effective anticancer agent led to the onset of clinical studies of

* Corresponding author. Tel.: +55 31 34095740; fax: +55 31 34095700.
E-mail address: hberaldo@ufmg.br (H. Beraldo).

0968-0896/$ - see front matter © 2012 Elsevier Ltd. All rights reserved.
http://dx.doi.org/10.1016/j.bmc.2012.04.027

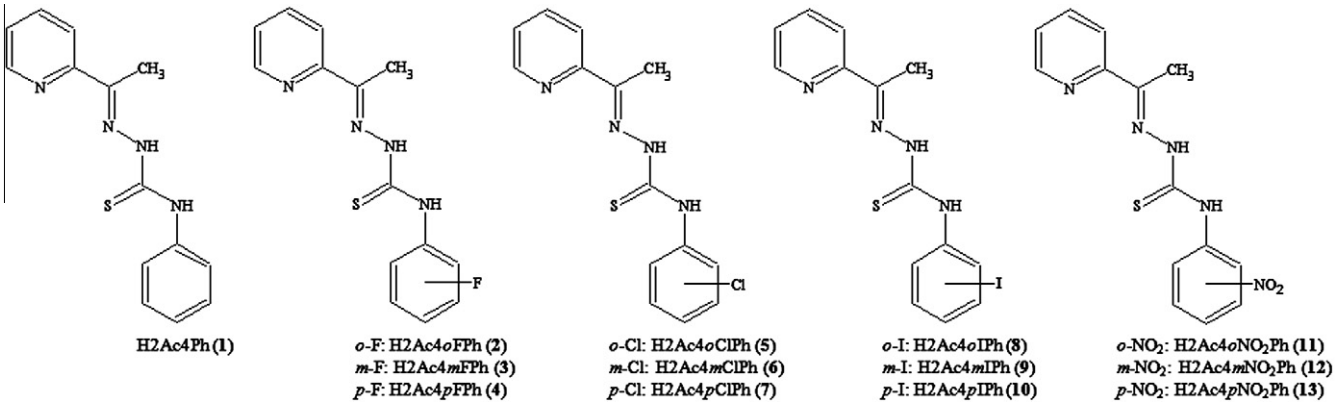

Figure 1. Structural representation of **1** (H2Ac4Ph), **2** (H2Ac4*o*FPh), **3** (H2Ac4*m*FPh), **4** (H2Ac4*p*FPh), **5** (H2Ac4*o*ClPh), **6** (H2Ac4*m*ClPh), **7** (H2Ac4*p*ClPh), **8** (H2Ac4*o*IPh), **9** (H2Ac4*m*IPh), **10** (H2Ac4*p*IPh), **11** (H2Ac4*o*NO_2Ph), **12** (H2Ac4*m*NO_2Ph), **13** (H2Ac4*p*NO_2Ph).

3-aminopyridine-2-carboxaldehyde thiosemicarbazone (3-AP; Triapine®, Vion Pharmaceuticals Inc., New Haven, CT).[12,13] The antitumor activity of α(N)-heterocyclic thiosemicarbazones has been attributed to their ability to inhibit ribonucleoside diphosphate reductase (RDR), a rate-limiting enzyme in DNA syntheses that catalyzes the conversion of ribonucleotides into deoxyribonucleotides.[11–14]

The cytotoxic activity of thiosemicarbazones and their metal complexes against a variety of human solid tumor cell lines as well as leukemic cells has been reported by other authors[15–19] and by our group.[20–24] Particularly, we have recently demonstrated that **1** (H2Ac4Ph) and its N^4-*ortho*-, -*meta*- and -*para*-chlorophenyl and N^4-*ortho*-, -*meta*- and -*para*-tolyl derivatives showed cytotoxicity at nanomolar concentrations against malignant glioma.[25] **1** and its chlorophenyl-derivatives were highly active against glioblastoma, and these results encouraged us to further investigate their cytotoxic properties as well as those of novel derivatives.[25]

The development of anticancer drugs requires the evaluation of the possible mechanism of action involved in the process of cancer cell death. During the past decade, advances in chemotherapy in order to induce apoptosis in cancer cells were achieved. More recently, the focus of the research has been on the non-apoptotic types of programmed cell death, such as autophagy, which is characterized by an increase in the number of autophagosomes, vesicles that surround cellular organelles.[26] Subsequently, autophagosomes merge with lysosomes and digest the organelles, leading to cell death.[27]

Apoptosis and autophagy are predominantly distinct. However, several studies have demonstrated cross-talk between them.[26] A

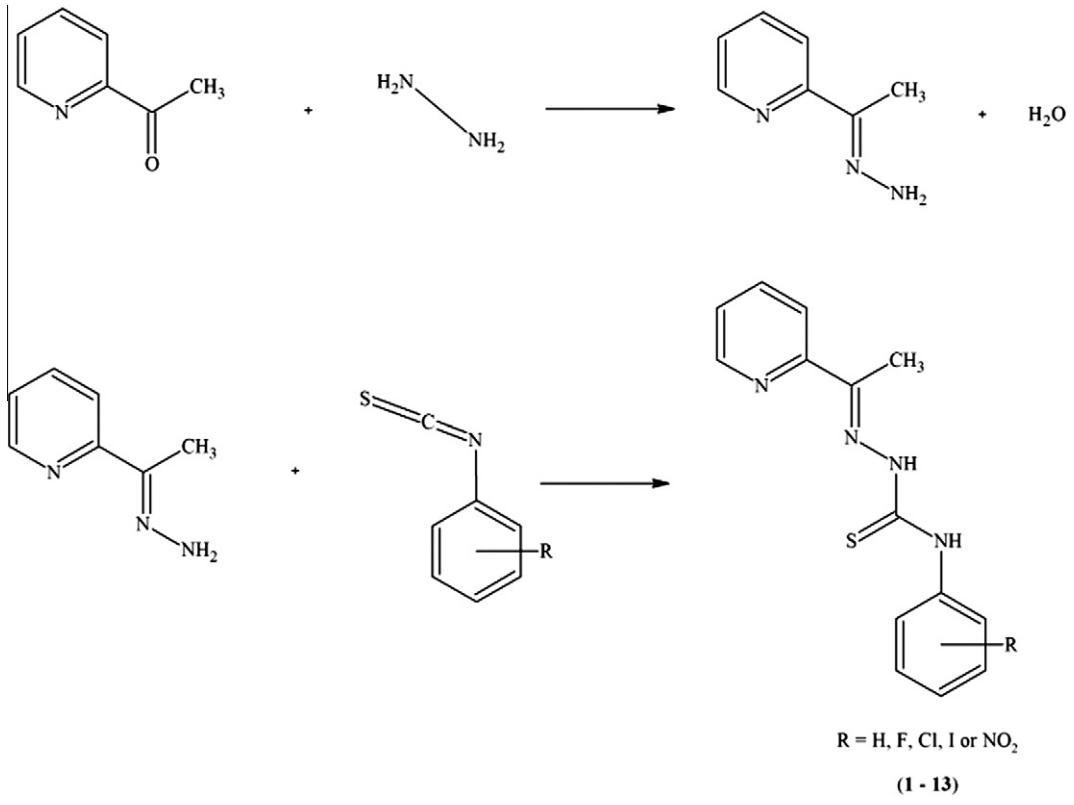

Scheme 1. Synthesis of compounds **1**-**13**.

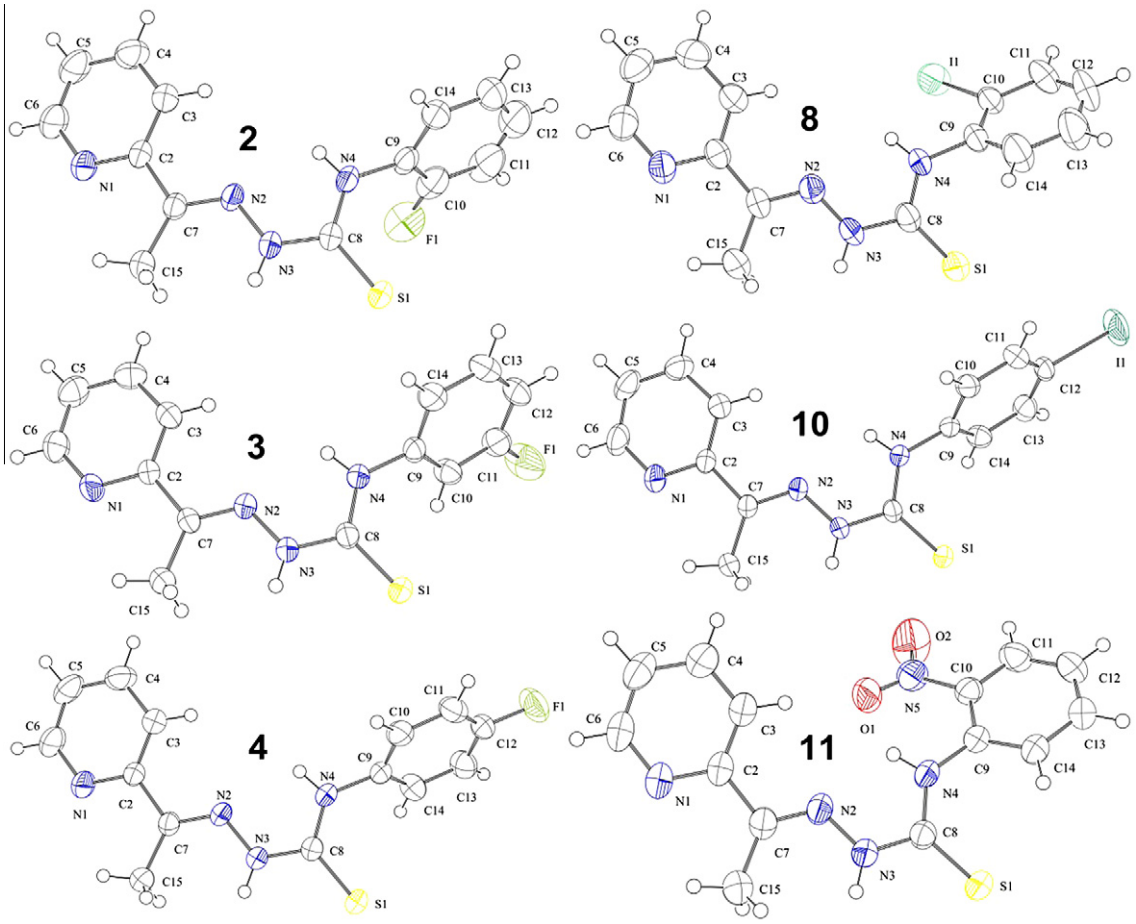

Figure 2. Molecular plots of **2**, **3**, **4**, **8**, **10** and **11** showing the labelling scheme of the non-H atoms and their displacement ellipsoids at the 50% probability level.

variety of chemotherapeutic agents (alkylating agents and arsenic trioxide), hormonal therapies (tamoxifen and vitamin D analogues), natural compounds (resveratrol), cytokines (IFNγ), gene therapies (p53 and p27Kip1), microtubule disturbing agents and radiotherapy have shown to trigger autophagic cell death in a panel of cancer cells.[28]

In the present work we evaluated the cytotoxicities of N^4-phenyl 2-acetylpyridine thiosemicarbazone (H2Ac4Ph; *N*-(phenyl)-2-(1-(pyridin-2-yl)ethylidene)hydrazinecarbothioamide) (**1**) and its N^4-*ortho*-, -*meta*- and -*para*-fluorophenyl (H2Ac4*o*FPh, H2Ac4*m*FPh, H2Ac4*p*FPh) (**2**–**4**), N^4-*ortho*-, -*meta*- and -*para*-chlorophenyl (H2Ac4*o*ClPh, H2Ac4*m*ClPh, H2Ac4*p*ClPh) (**5**–**7**), N^4-*ortho*-, -*meta*- and -*para*-iodophenyl (H2Ac4*o*IPh, H2Ac4*m*IPh, H2Ac4*p*IPh) (**8**–**10**) and N^4-*ortho*-, -*meta*- and -*para*-nitrophenyl (H2Ac4*o*NO_2Ph, H2Ac4*m*NO_2Ph, H2Ac4*p*NO_2Ph) (**11**–**13**) derivatives (Fig. 1) against MCF-7 (breast adenocarcinoma), U87 (glioblastoma multiforme expressing wild-type p53 protein) and T98G (glioblastoma multiforme expressing mutant p53) human malignant tumor cells. A preliminary analysis of the compounds' mechanism of action was carried out along with structure–activity relationship (SAR) studies. The effect of H2Ac4*p*ClPh on tubulin assembly and its effects on cellular microtubule organization and mitotic arrest were also investigated.

2. Results and discussion

2.1. Formation of the thiosemicarbazones

Preparation of all thiosemicarbazones was carried out by a previously described method,[29] as shown in Scheme 1. The novel thiosemicarbazones **8**–**10** were characterized by means of their infrared, NMR and HRMS spectra.

2.2. Characterization of the thiosemicarbazones

In the infrared spectra of **8**–**10** vibrations attributed to ν(N–H) at 3306–3264 and 3232–3208 cm^{-1} were observed. Absorptions at 1595–1581 and 786–782 cm^{-1} were attributed to ν(C=N) and ν(C=S), respectively. Absorptions attributed to the in-plane deformation mode of the pyridine ring were observed at 621–616 cm^{-1}.

Duplicated signals were observed in the ^{1}H NMR spectra (DMSO-d_6) of **8**–**10** suggesting a mixture of the *E* (95–87%) and *Z* (13–5%) configurational isomers. This behavior has also been observed for other 2-acetylpyridine-derived thiosemicarbazones.[25] The N^3–H chemical shifts at δ 10.90–10.79 ppm, are characteristic of the *E* configuration, in which N^3–H is hydrogen bonded to the solvent,[20–22] while chemical shifts at δ 14.69–14.66 ppm indicate the presence of the *Z* configuration, in which N^3–H is hydrogen bonded to the pyridine nitrogen.[20–22] Some hydrogen signals of the *Z* isomer could not be observed separately since they appear in the same region as those of the *E* isomer.

2.3. X-ray diffraction analysis

Upon slow evaporation in 9:1 acetone/DMSO crystals of **2**–**4**, **8**, **10** and **11** were formed and their crystal structures were determined by X-ray diffraction. The crystal structures of **1**[30] and **5**–**7**[25] had been previously determined.

Figure 2 shows perspective views of **2**–**4**, **8**, **10** and **11**. Table 1 reports the crystal data and refinement results for the determined

Table 1
Crystal data and refinement results for **2**–**4**, **8**, **10** and 11

Compound		**2**	**3**	**4**	**8**	**10**	11
Empirical formula		$C_{14}H_{13}FN_4S$	$C_{14}H_{13}FN_4S$	$C_{14}H_{13}FN_4S$	$C_{14}H_{13}IN_4S$	$C_{14}H_{13}IN_4S$	$C_{14}H_{13}N_5O_2S$
Formula weight		288.34	288.34	288.34	396.24	396.24	315.35
Crystal system		Monoclinic	Triclinic	Triclinic	Monoclinic	Monoclinic	Monoclinic
Space group		*P* 21/c	*P* $\bar{1}$	*P* $\bar{1}$	*P* 21/*n*	*P* 21/*n*	P 21/*c*
Unit cell dimensions	a, Å	5.4620(2)	5.8660(4)	5.8396(4)	11.3298(3)	10.4026(3)	11.3298(3)
	b, Å	10.5664(4)	10.1714(6)	10.2292(6)	7.5376(2)	5.6886(2)	7.5376(2)
	c, Å	24.1928(9)	12.0075(7)	11.8164(7)	17.2904(5)	25.9488(6)	17.2904(5)
	α, °	90	75.061(5)	76.218(5)	90	90	90
	β, °	94.868(3)	85.873(5)	87.761(5)	98.910(3)	92.499(2)	98.910(4)
	γ, °	90	89.139(5)	89.358(5)	90	90	90
Volume, Å^3		1391.22(9)	690.42(7)	685.00(7)	1529.08(11)	1534.09(8)	1458.77(7)
Z/density calcd, Mg/m^3		4/1.377	2/1.387	2/1.398	4/1.721	4/1.716	4/1.436
Absorption coefficient, mm^{-1}		0.239	0.241	0.243	2.226	2.219	0.237
F(000)		600	300	300	776	776	656
Crystal size, mm		0.20 × 0.12 × 0.06	0.23 × 0.16 × 0.12	0.25 × 0.12 × 0.08	0.36 × 0.20×0.10	0.39 × 0.20 × 0.07	0.23 × 0.17 × 0.08
θ range for data coll., °		3.19–26.37	4.10–26.37	3.02–26.37	2.76–26.37	3.00–26.37	2.77–26.37
Index range		$-6 \leqslant h \leqslant 6$	$-7 \leqslant h \leqslant 6$	$-7 \leqslant h \leqslant 6$	$-15 \leqslant h \leqslant 14$	$-11 \leqslant h \leqslant 13$	$-14 \leqslant h \leqslant 13$
		$-9 \leqslant k \leqslant 13$	$-12 \leqslant k \leqslant 11$	$-12 \leqslant k \leqslant 12$	$-5 \leqslant k \leqslant 5$	-6 ⩽ *k* ⩽ 7	$-9 \leqslant k \leqslant 9$
		$-25 \leqslant l \leqslant 3$	$-14 \leqslant l \leqslant 11$	$-14 \leqslant l \leqslant 10$	$-34 \leqslant l \leqslant 34$	$-31 \leqslant l \leqslant 32$	$-20 \leqslant l \leqslant 21$
Collected reflections/unique (R_{int})		10392/2834(0.0605)	4972/2809(0.0353)	5207/2804(0.0278)	9035/3120(0.0325)	13323/3120(0.0598)	11910/2987(0.0371)
Completeness (%)		99.9 (to 26.37°)	99.6 (to 26.37°)	99.9 (to 26.37°)	99.9 (to 26.37°)	99.9 (to 26.37°)	99.9 (to 26.37°)
Max and min transmission		0.9858 and 0.9538	0.9717 and 0.9467	0.9811 and 0.9660	1.00000 and 0.77529	0.8784 and 0.4782	0.9813 and 0.9475
Data/restraints/parameters		2834/0/182	2809/0/182	2804/0/182	3120/0/182	3120/0/182	2966/0/200
Goodness-of-fit on F^2		0.987	1.063	0.915	0.887	1.053	1.061
Final *R* indices [$I > 2\sigma(I)$]		R_1 = 0.0422	R_1 = 0.0480	R_1 = 0.0379	R_1 = 0.0323	R_1 = 0.0392	R_1 = 0.0369
		wR_2 = 0.1155	wR_2 = 0.1425	wR_2 = 0.0846	wR_2 = 0.0658	wR_2 = 0.1096	wR_2 = 0.0990
R indices (all data)		R_1 = 0.0601	R_1 = 0.0645	R_1 = 0.0660	R_1 = 0.0607	R_1 = 0.0511	R_1 = 0.0540
		wR_2 = 0.1293	wR_2 = 0.1495	wR_2 = 0.0901	wR_2 = 0.0706	wR_2 = 0.1140	wR_2 = 0.1039
Largest peak & hole, e Å^{-3}		0.300/−0.326	0.598/−0.279	0.219/−0.178	0.607/−0.706	1.066/−1.246	0.161/−0.206

structures. Selected intra-molecular bond distances and angles for **1**[30] and **5**–**7**,[25] **2**–**4**, **8**, **10** and **11** are given in Tables 2 and 3, respectively.

The bond distances are very similar in all structures. The S1–C8 bond varies from 1.654(3) to 1.677(2) Å. This bond is longer in **1** than in its derivatives. The C2–C7 bond varies from 1.472(4) to 1.497(2) Å. The N2–C7, N2–N3, N4–C8 and N4–C9 bonds are in the 1.278(2)–1.290(3) Å, 1.361(3)–1.378(3) Å, 1.328(4)–1.3514(19) Å and 1.3973(19)–1.430(3) Å ranges, respectively. Compound **11** has the shortest N4–C9 bond, which can be attributed to the resonance withdrawing effect of the *ortho* nitro group. In general the bond distances in the thiosemicarbazone skeleton of **11** were shorter than in the other derivatives (see Table 2).

As expected, in all thiosemicarbazones the bond angles are also similar, but some differences were observed for the N4–C8–N3, N4–C8–S1, C7–N2–N3 and C8–N4–C9 bond angles in **11** in comparison with the other thiosemicarbazones (see Table 3). These differences might be attributed to a geometric constraint due to the formation of an additional N4H···O2 intra-molecular hydrogen bond observed in the structure of **11** (see Table 4) which is absent in thiosemicarbazones **2**–**4**, **8** and **10**.

All thiosemicarbazones **2**–**4**, **8**, **10** and **11** adopt the *EE* conformation in relation to the C7–N2 and N3–C8 bonds. The presence of the *E* conformation with respect to the N3–C8 bond, commonly observed in the solid state, is associated with the formation of a pair of N–H···S hydrogen bonds that are interrelated across a center of inversion generating dimmers.[25] As can be seen in Table 4, all the NH···S interactions are linked to a symmetry operation. A weak N4–H···N2 intra-molecular hydrogen bond (see Table 4) is present in all structures, except in **8**. This hydrogen bond probably hinders rotation around the N3–C8 bond and might contribute to the stability of the *EE* conformation. Fig. 3 shows the packing of **3** and **11**, with the inter-molecular N–H···S hydrogen bonds.

2.4. Cytotoxic activity against malignant breast and glioma cells

The results showed that all thiosemicarbazones were cytotoxic in a dose-dependent way against all studied tumor cell lineages (Supporting Material). The concentrations that inhibit 50% of cell survival (IC_{50}) (Table 5) were found in the 52–0.16, 140–1.0, and 160–1.4 nM ranges for MCF-7, T98G and U87 cells, respectively. Breast tumor cells were significantly more sensitive to the thiosemicarbazones' cytotoxic effect than glioma cells. However, there was no significant difference between their cytotoxic effect against U87 and T98G cells, suggesting that the mutation extent in the p53 gene of T98G cells did not interfere in the thiosemicarbazones' cytotoxic effect.

Although in general the presence of substituents on the N^4-phenyl group does not lead to more cytotoxic compounds, in some cases the substituted derivatives were as or more potent than **1**. Thus, in these cases the presence of different substituents was an interesting strategy to improve the cytotoxicity of **1**. Generally, the *ortho* substituted thiosemicarbazones were more active against the three cell lines than their *meta* and *para* position isomers.

All thiosemicarbazones presented higher cytotoxic activity than the topoisomerase II inhibitor etoposide for which the IC_{50} values were 480, 460 and 620 nM against MCF-7, T98G and U87 cells, respectively. Moreover, the thiosemicarbazones' antitumoral doses resulted in no significant toxicity to red blood cells (IC_{50} >10^{-5} M), indicating a good therapeutic index.

2.5. SAR studies

SAR studies were carried out to identify the stereo and electronic properties determined by theoretical calculations that may be involved in the mechanism of action of **1**–**13**. Properties of interest in this study were molecular surface area, theoretical octanol–water

Table 2
Selected bond distances (Å) for **1** and its derivatives

Atoms	**1**[30]	**5**[25,a]		**6**[25]	**7**[25]	**2**	**3**	**4**	**8**	**10**	**11**
S1–C8	1.677(2)	1.654(3)	1.654(3)	1.669(3)	1.671(2)	1.6711(17)	1.671(2)	1.672(2)	1.665(3)	1.670(3)	1.6613(15)
C2–C7	1.486(2)	1.474(4)	1.472(4)	1.487(4)	1.484(2)	1.488(2)	1.487(3)	1.487(2)	1.473(5)	1.495(4)	1.497(2)
N2–C7	1.284(3)	1.281(3)	1.278(3)	1.290(3)	1.283(2)	1.283(2)	1.287(3)	1.280(2)	1.285(4)	1.285(4)	1.278(2)
N2–N3	1.376(2)	1.362(3)	1.361(3)	1.378(3)	1.374(2)	1.3783(19)	1.371(2)	1.377(2)	1.368(4)	1.376(3)	1.3681(18)
N3–C8	1.358(3)	1.359(3)	1.351(3)	1.354(3)	1.352(2)	1.346(2)	1.359(3)	1.349(2)	1.361(4)	1.352(4)	1.361(2)
N4–C8	1.346(3)	1.328(4)	1.336(3)	1.349(3)	1.341(2)	1.343(2)	1.340(3)	1.342(2)	1.336(4)	1.347(4)	1.3514(19)
N4–C9	1.421(3)	1.413(3)	1.421(3)	1.430(3)	1.423(2)	1.412(3)	1.421(3)	1.428(2)	1.419(4)	1.417(4)	1.3973(19)
C–R[b]	—	1.679(11) 1.800(14)	1.724(3)	1.741(3)	1.7411(19)	1.347(3)	1.352(3)	1.362(2)	2.088(3)	2.087(3)	1.456(2)

[a] There are two molecules in the asymmetric unit.
[b] R = F, Cl, I or NO_2.

Table 3
Selected angles for **1** and its derivatives

Atoms	**1**[30]	**5**[25,a]		**6**[25]	**7**[25]	**2**	**3**	**4**	**8**	**10**	**11**
N2N3C8	118.9(2)	118.2(2)	118.9(2)	119.0(2)	118.66(15)	118.14(14)	118.67(17)	119.18(14)	119.1(3)	118.7(2)	118.23(13)
N3C8S1	119.7(1)	121.0(2)	121.5(2)	121.2(2)	119.99(15)	121.12(13)	119.93(15)	120.19(12)	120.7(2)	120.2(2)	120.70(11)
N4C8N3	114.8(2)	114.7(2)	114.4(2)	114.4(2)	114.71(17)	114.99(15)	114.43(17)	114.58(15)	114.9(3)	114.9(2)	112.28(13)
N4C8S1	125.5(2)	124.3(2)	124.1(2)	124.3(2)	125.26(14)	123.88(14)	125.60(15)	125.22(13)	124.5(2)	124.9(2)	126.99(13)
C7N2N3	118.8(2)	119.1(2)	118.7(2)	118.7(2)	118.86(15)	118.79(14)	118.37(18)	118.91(13)	118.9(3)	118.1(2)	121.28(14)
C8N4C9	127.6(2)	125.1(3)	123.5(2)	125.4(2)	126.87(17)	125.95(15)	127.40(17)	127.07(14)	125.2(3)	126.5(2)	129.92(13)

[a] There are two molecules in the asymmetric unit.

Table 4
Hydrogen bonds [Å and °] for **2–4**, **8**, **10** and **11**

Compound	D—H···A	d(D—H)	d(H···A)	d(D···A)	(D—H···A)	Symmetry operation
2	N4—H4···N2	0.86	2.16	2.568(2)	108.6	—
	N3—H3···S1	0.86	2.72	3.5798(16)	174.4	−x+2,−y+1,−z+1
3	N4—H4···N2	0.86	2.16	2.580(2)	109.5	—
	N3—H3···S1	0.86	2.87	3.7215(18)	172.8	−x,-y+1,−z+2
4	N4—H4···N2	0.86	2.16	2.583(2)	110.1	—
	N3—H3···S1	0.86	2.87	3.7289(15)	174.5	−x,-y+1,−z+1
8	N3—H3A···S1	0.86	2.78	3.635(3)	171.0	−x+1,−y+1,−z
10	N4—H4···N2	0.86	2.17	2.586(3)	109.1	—
	N3—H3A···S1	0.86	2.80	3.652(3)	173.8	−x+1,−y+2,−z+1
11	N4—H4···N2	0.86	2.05	2.5208(19)	113.4	—
	N3—H3A···S1	0.86	2.79	3.6383(14)	167.9	−x+1,−y+2,−z
	N4—H4···O1	0.86	2.06	2.6137(17)	121.8	—

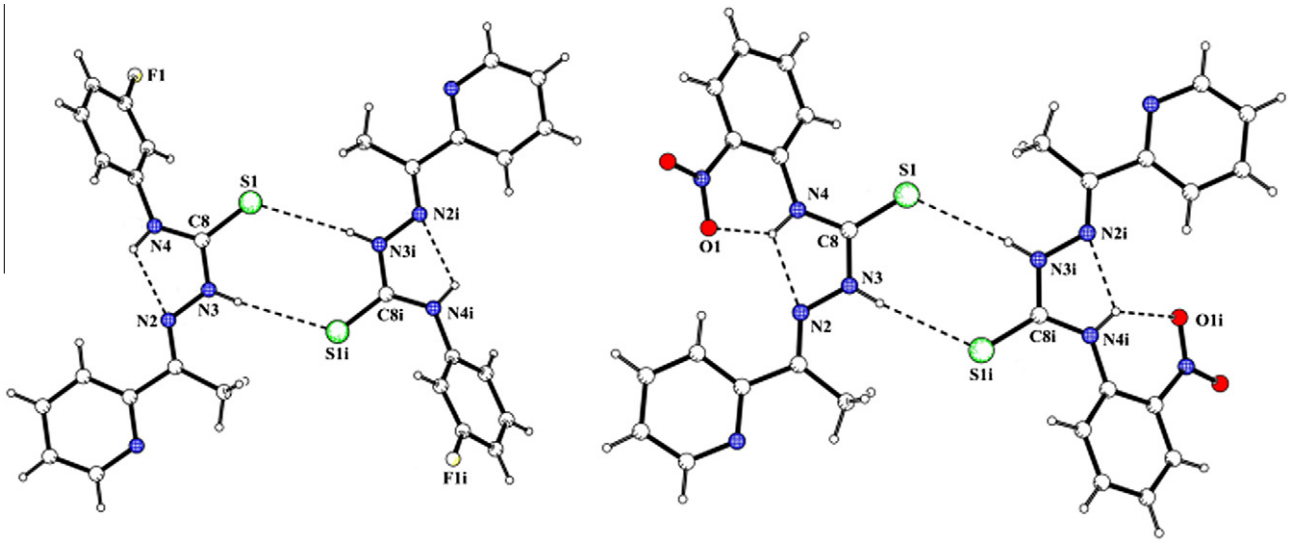

Figure 3. Molecular packing of **3** (left) and **11** (right), showing the N–H···S hydrogen bond (dashed lines).

Table 5
Cytotoxic effect of **1–13** and etoposide on malignant cells and their haemolytic activity

Compound	IC_{50} (nM)[a]			Haemolytic activity (nM)[b]
	MCF-7	T98G	U87	
1	0.18 ± 0.06	6.80 ± 0.83	1.40 ± 0.39	>10000
2	0.39 ± 0.20	3.10 ± 2.20	5.00 ± 0.47	>10000
3	9.00 ± 2.00	12.00 ± 5.40	18.00 ± 1.70	>10000
4	1.20 ± 0.73	17.00 ± 1.90	10.00 ± 10.00	>10000
5	0.16 ± 0.14	1.10 ± 0.96	2.60 ± 2.10	>10000
6	24.00 ± 1.50	1.00 ± 0.40	31.00 ± 9.60	>10000
7	8.50 ± 0.40	5.90 ± 0.76	1.70 ± 0.82	>10000
8	4.10 ± 1.90	8.10 ± 4.20	6.10 ± 2.10	>10000
9	45.00 ± 37.00	61.00 ± 25.00	84.00 ± 10.00	>10000
10	6.60 ± 3.20	64.00 ± 36.00	59.00 ±37.00	>10000
11	5.70 ± 0.19	6.60 ± 3.30	4.30 ± 0.82	>10000
12	38.00 ± 32.00	140.00 ± 110.00	69.00 ± 7.10	>10000
13	52.00 ± 21.00	140.00 ± 11.00	160.00 ± 56.00	>10000
Etoposide	480.00 ± 70.00	460.00 ± 25.00	620.00 ± 150.00	

[a] IC_{50} determined by the MTT assay.
[b] IC_{50} determined by direct haemolysis assay. Data were expressed as average ± standard deviation, $n = 4$.

partition coefficients (log*P*), dipole moment, highest occupied molecular orbital (HOMO) and lowest unoccupied molecular orbital (LUMO) energies, which were correlated to pIC_{50} ($-\log IC_{50}$). Molecular surface area may offer information on stereo features for drug–receptor interactions. Log*P* and dipole values may give some insights on the degree of lipophilicity of these molecules. Additionally, HOMO and LUMO energies are related to ionization potential and electron affinity, respectively. These frontier orbitals are associated to the molecule's reactivity. HOMO energy is closely related to susceptibility to electrophilic attack while LUMO energy is closely related to susceptibility to nucleophilic attack.

Calculated stereo and electronic properties for **1–13** and experimental pIC_{50} values against MCF-7, T98G and U87 cells are shown in Table 6. Attempting to establish some correlation between stereo-electronic parameters and biological activity, we built simple correlation matrices (Supporting Material) for the *E* and *Z* isomers.

SAR data for the *E* isomers indicate that there are similar correlations between the chemical descriptors and cytotoxic activity against MCF-7 and U87 cells. Different correlations were found between descriptors and cytotoxicity against T98G and U87 cells. Although U87 and T98G are both glioma cells, the former is wild-type while the latter is a p53-mutant cell. Thus, the mechanisms of thiosemicarbazones' cytotoxic action may be different in these two cell lines. Reasonable correlations were observed between the cytotoxic activities against MCF-7 and U87 cells and the molecular surface area ($R = -0.71$ and -0.60 for MCF-7 and U87 cells, respectively), the HOMO energy ($R = 0.69$ and 0.67 for MCF-7 and U87 cells, respectively) and the charge on sulfur ($R = 0.71$ and 0.68 for MCF-7 and U87 cells, respectively). Thus,

Table 6
Experimental pIC_{50} ($-\log IC_{50}$) values for **1–13** against MCF-7, T98G and U87 cells and calculated stereo and electronic properties

Compound		pIC_{50} MCF-7	pIC_{50} T98G	pIC_{50} U87	Surface area (Å)	HOMO (eV)	LUMO (eV)	Log*P* (ALOGPs)	Dipole (*D*)	Charge (e. u.)[a]		
										N_{py}	N_{azo}	S
E Isomers	1	9.745	8.167	8.854	365.315	−8.171	1.690	3.100	5.281	−0.484	−0.296	−0.200
	2	9.409	8.509	8.301	371.197	−8.307	1.650	3.220	4.211	−0.485	−0.296	−0.198
	3	8.046	7.921	7.745	372.401	−8.400	1.520	3.240	4.496	−0.484	−0.297	−0.193
	4	8.921	7.770	8.000	372.370	−8.283	1.536	3.230	5.795	−0.483	−0.297	−0.201
	5	9.796	8.959	8.585	380.124	−8.346	1.621	3.670	3.877	−0.485	−0.293	−0.196
	6	7.620	9.000	7.509	382.152	−8.416	1.509	3.650	4.374	−0.484	−0.298	−0.192
	7	8.071	8.229	8.770	382.175	−8.304	1.492	3.650	6.042	−0.483	−0.298	−0.195
	8	8.387	8.092	8.215	390.191	−8.332	1.612	3.780	4.437	−0.485	−0.290	−0.196
	9	7.347	7.215	7.076	391.944	−8.407	1.510	3.790	4.651	−0.484	−0.297	−0.193
	10	8.180	7.194	7.229	391.979	−8.220	1.483	3.800	5.788	−0.483	−0.297	−0.195
	11	8.244	8.180	8.367	402.386	−8.370	0.840	3.170	1.826	−0.489	−0.287	−0.192
	12	7.420	6.854	7.161	406.617	−8.602	1.225	3.170	4.174	−0.484	−0.300	−0.188
	13	7.284	6.854	6.796	406.613	−8.688	1.096	3.180	7.978	−0.483	−0.299	−0.178
Z Isomers	1	9.745	8.167	8.854	364.729	−7.916	1.466	3.100	6.968	−0.503	−0.290	−0.201
	2	9.409	8.509	8.301	370.528	−8.063	1.469	3.220	6.024	−0.503	−0.288	−0.201
	3	8.046	7.921	7.745	371.803	−8.152	1.371	3.240	7.161	−0.503	−0.291	−0.194
	4	8.921	7.770	8.000	371.781	−8.030	1.395	3.230	8.186	−0.503	−0.291	−0.203
	5	9.796	8.959	8.585	379.517	−8.107	1.448	3.670	5.864	−0.503	−0.286	−0.196
	6	7.620	9.000	7.509	381.567	−8.169	1.359	3.650	7.277	−0.503	−0.292	−0.194
	7	8.071	8.229	8.770	381.574	−8.060	1.352	3.650	8.704	−0.503	−0.292	−0.197
	8	8.387	8.092	8.215	389.019	−8.119	1.437	3.780	6.278	−0.503	−0.283	−0.194
	9	7.347	7.215	7.076	391.345	−8.160	1.358	3.790	7.231	−0.503	−0.291	−0.195
	10	8.180	7.194	7.229	391.425	−7.998	1.343	3.800	8.103	−0.503	−0.291	−0.196
	11	8.244	8.180	8.367	403.070	−8.258	1.078	3.170	4.617	−0.504	−0.279	−0.190
	12	7.420	6.854	7.161	406.006	−8.390	1.228	3.170	8.250	−0.504	−0.293	−0.190
	13	7.284	6.854	6.796	405.998	−8.473	1.077	3.180	11.486	−0.504	−0.292	−0.179

[a] e. u.: electrostatic unit.

the smaller the molecular surface area, the higher the cytotoxic activity against MCF-7 and U87 cells. A direct correlation was found between the HOMO energies and the activities against MCF-7 and U87 cells, which is an interesting result since the HOMO energy is closely related to the molecules' reactivity. Besides, the direct correlation between cytotoxicity and the charge on sulfur indicates that the more negatively charged the sulfur atom, the higher anti-proliferative effect of the thiosemicarbazones against MCF-7 and U87 cells. It's noteworthy that HOMO energy and negative charge on sulfur are correlated ($R = 0.90$) and both properties are correlated to the activities against MCF-7 and U87 cells. Thus, the sulfur atom may play an important role in the thiosemicarbazones' reactivity and therefore, in their cytotoxic activity.

Comparison of HOMO density plots for all *E* isomers (Fig. 4) shows distinct electronic delocalization among the studied thiosemicarbazones, which may partially account for the difference in biological activity of these compounds, although other parameters may not be excluded.

Concerning correlation between the properties of *E* isomers and activity against T98G cells, we only found an inverse correlation between cytotoxicity and molecular surface area ($R = -0.60$).

The same correlations observed for *E* isomers were also verified for the *Z* isomers. In addition, for the *Z* isomers the cytotoxic activity against T98G cells is correlated to the LUMO energy ($R = 0.63$) and the dipole ($R = 0.62$).

2.6. Morphological analysis of tumor cells

Treatment with compounds **1**–**13** induced visible membrane and nuclear alterations characteristics of programmed cell death on breast and glioma cells. The main morphological changes observed were: irregularities in cellular shape, cell shrinkage and membrane blebbing (Fig. 5). Moreover, chromatin condensation and DNA fragmentation were observed in all treated cells when stained with 4′,6-diamidine-2-phenylindole dihydrochloride (DAPI) (Fig. 6). These results suggest that the reduction of cell survival after treatment with thiosemicarbazones occurred, at least in part, due to apoptosis induction.

Although DAPI is a commonly used assay for detection of apoptosis, this method cannot rule out other kinds of cell death and it is very important to analyze cell death using other fluorescent DNA binding dyes as acridine orange/ethidium bromide.[31]

Figures. 5 and 6 show, as examples, breast and glioma cells treated with compound **7**.

2.7. Acridine orange–ethidium bromide (AO/EB) double staining assay

Acridine orange/ethidium bromide (AO/EB) staining can be used to differentiate live, apoptotic and necrotic cells. Moreover, acridine staining is very useful to show cytoplasmic acidic vacuoles characteristics of autophagy. Under AO/EB staining untreated control breast and glioma cells showed cytoplasm and nucleus with homogeneous green with minimal orange fluorescence indicative of healthy cells. On the other hand, cells treated with the thiosemicarbazones presented chromatin condensation, visible as bright green fragments, and absence of EB fluorescence, indicating preserved membrane. All of these characteristics are typical of early apoptosis. Moreover, treated cells presented large acidic compartments in the cytoplasm, and visible red fluorescence suggesting the presence of autophagolysosomes, considered a characteristic feature of cells engaged in autophagy.[32] However, more specific tests, like the quantification of mammalian autophagy protein (LC3),[33] are necessary to confirm this hypothesis. Further studies should be performed in order to determine the exact mechanism of cell death triggered by these compounds.

Chemotherapeutics like cisplatin and etoposide can induce apoptosis and autophagy in tumor cells.[34,35] Taken together, our results suggest that, like cisplatin and etoposide, the studied

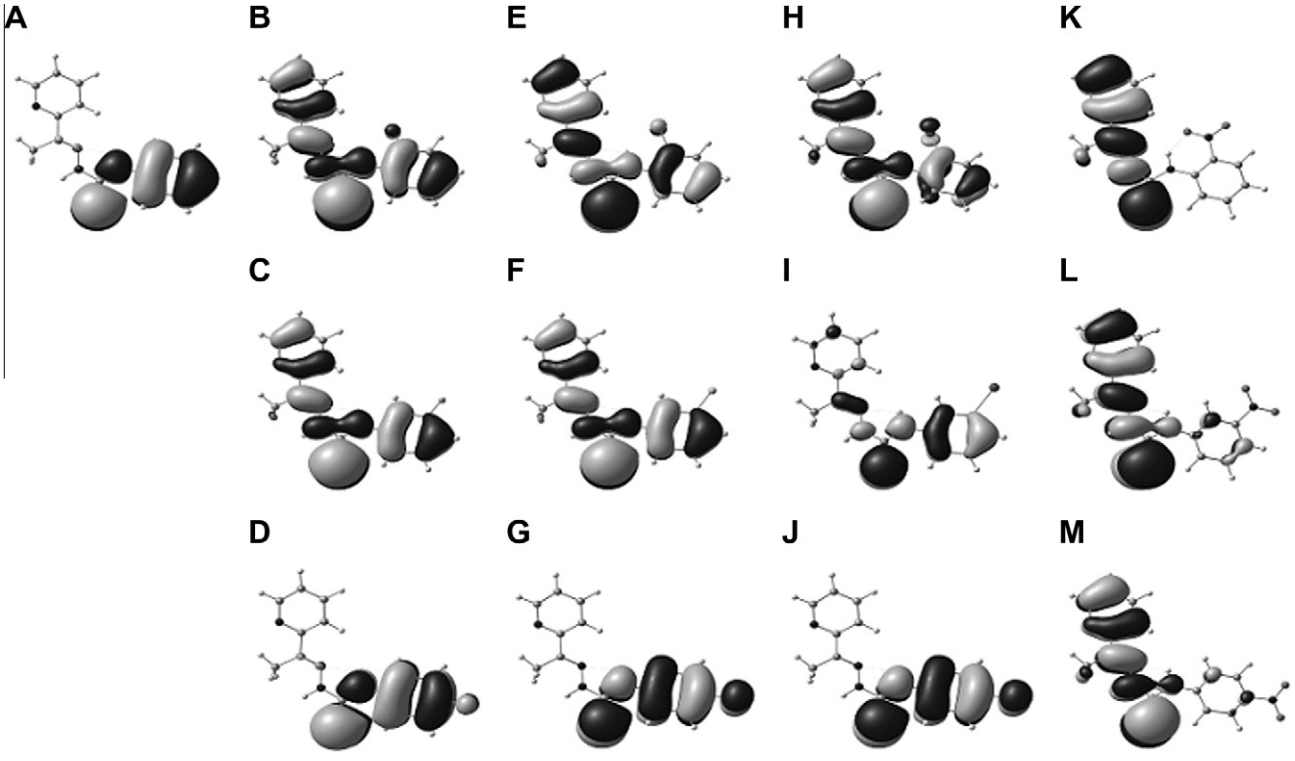

Figure 4. HOMO density distributions of: **1** (A), **2** (B), **3** (C), **4** (D), **5** (E), **6** (F), **7** (G), **8** (H), **9** (I), **10** (J), **11** (K), **12** (L) and **13** (M). Contour value = 0.018.

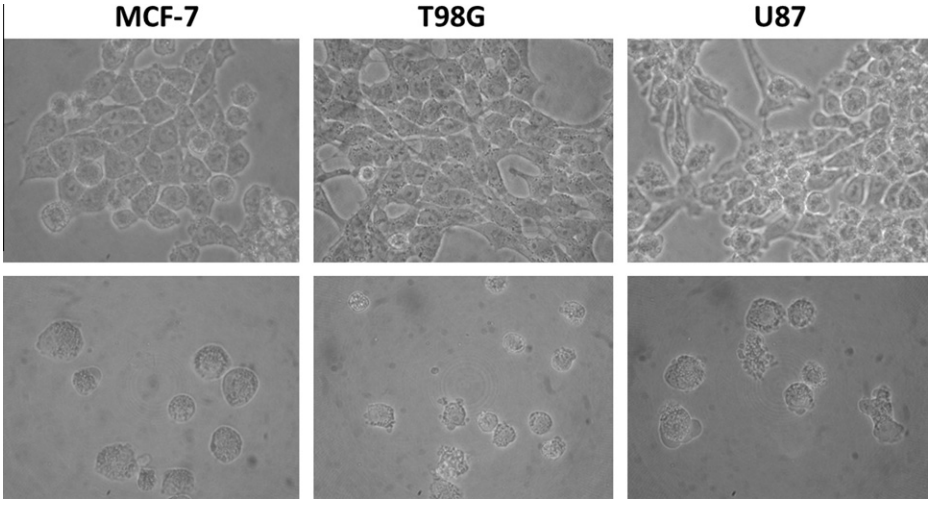

Figure 5. Compound **7** induces morphological changes on MCF-7 breast and T98G and U87 glioma tumor cell lines. Tumor cells were treated with **7** (1 μM) for 48 h. Cell shrinkage and irregularity in cellular shape were seen in cells treated with **7**. Photomicrographs from phase-contrast microscopy. Control cells are represented above and treated cells bellow. Magnification: 400×.

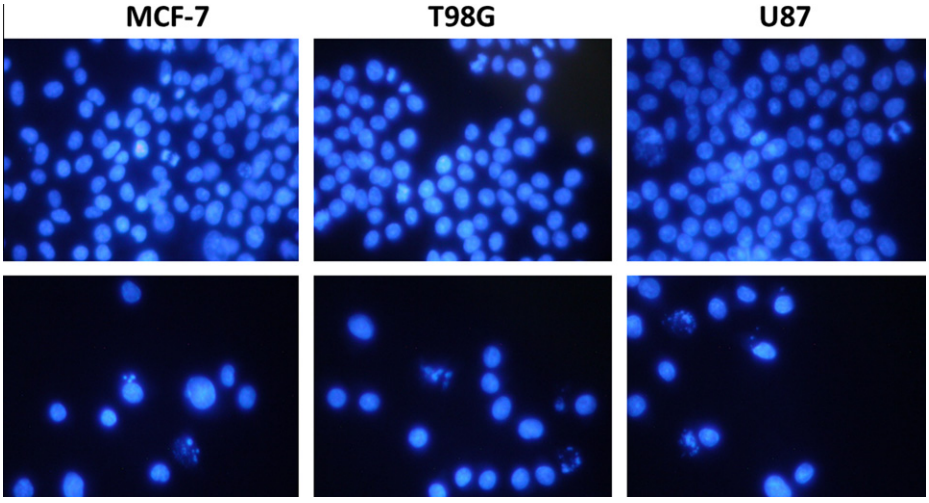

Figure 6. Compound **7** induces nuclear changes on MCF-7 breast and T98G and U87 glioma tumor cell lines. Tumor cells were treated with **7** (1 μM) for 48 h. After treatment cells were stained with DAPI. Nuclear condensation and formation of apoptotic bodies were seen in cells treated with **7**. Photomicrographs from fluorescence microscopy. Control cells are represented above and treated cells bellow. Magnification: 400×.

thiosemicarbazones were able to induce these two types of programmed cell death. Figure 7 shows, as example, breast and glioma cells treated with compound **7** and stained with acridine orange/ethidium bromide.

2.8. Effects on tubulin assembly

Interference with either assembly or disassembly of microtubules in rapidly dividing cells results in cell cycle arrest, triggering signals that induce apoptosis.[36] In light of the finding that cytotoxic thiosemicarbazones induce apoptosis, we investigated whether the mechanisms of either cytotoxicity or apoptosis were related to inhibition of tubulin assembly or microtubule stabilization. Four twofold concentrations of **7** were screened for their effects on *in vitro* tubulin polymerization (Fig. 8). As it can be seen, at high concentrations **7** seemed to cause a partial concentration-dependent inhibition of tubulin assembly. Although 2.5 μM of colchicine completely abolished tubulin polymerization, total inhibition of tubulin assembly in the presence of **7** was not observed even at concentrations close to the limit of solubility of the compound.

2.9. High content analysis of mitotic arrest

Microtubule interacting agents characteristically provoke cell cycle arrest and cellular microtubule perturbations.[37] The fact that **7** apparently inhibited *in vitro* polymerization of purified tubulin motivated the investigation on the effects of this compound on cellular microtubule perturbation and mitotic arrest. The cellular phenotypic changes associated with mitotic arrest caused by **7** were investigated as previously described.[37,38] Asynchronously growing HeLa cells were treated with the assayed compounds and incubated with primary antibodies for tubulin and the mitotic marker protein phosphohistone H3, followed by fluorescein-isothiocyanate (FITC) and Cy3-conjugated secondary antibodies, respectively. Cells were detected by nuclear counterstaining with Hoechst 33342, which also provided information about chromatin condensation and cell density as markers of cell death.

Please cite this article in press as: Soares, M. A.; et al. *Bioorg. Med. Chem.* (2012), http://dx.doi.org/10.1016/j.bmc.2012.04.027

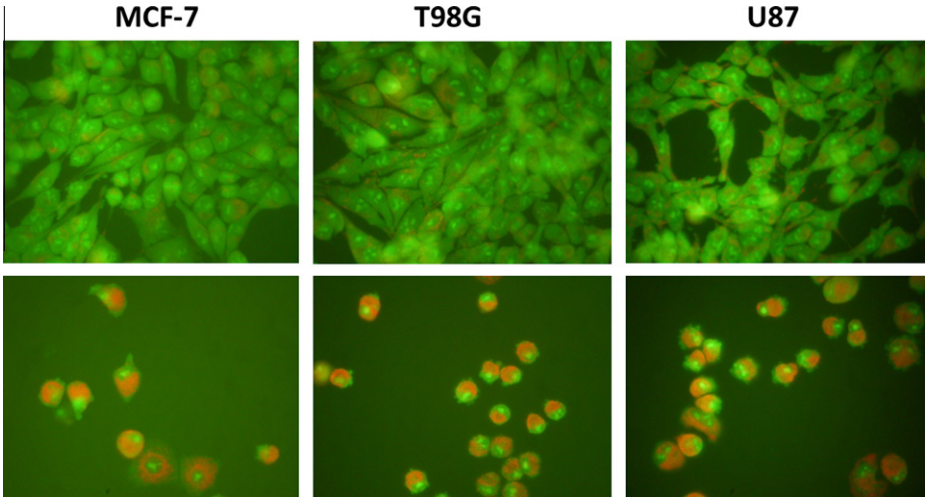

Figure 7. Detection of thiosemicarbazone-induced acidic autophagossomes and apoptosis. MCF-7 breast and T98G and U87 glioma tumor cell lines were treated with **7** (1 μM) for 48 h. After treatment cells were stained with acridine orange/ethidium bromide. Photomicrographs from fluorescence microscopy. Control cells are represented above and treated cells bellow. Magnification: 400×.

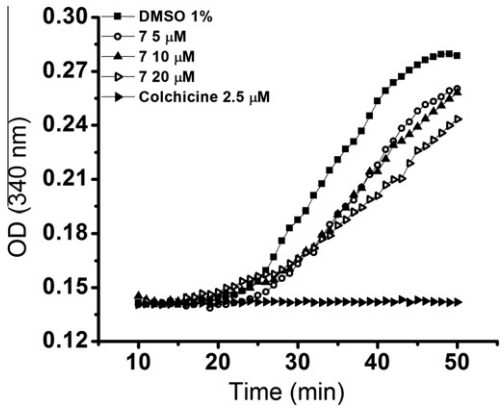

Figure 8. *In vitro* inhibition of tubulin assembly. Electrophoretically homogeneous bovine brain tubulin (final concentration 10 μM; 1 mg mL^{-1}) was pre-incubated with the studied compounds dissolved in DMSO (1% v/v final concentration) and monosodium glutamate (0.8 M final concentration) at 30 °C in 96-well plates. The reaction mixtures were cooled to 0 °C for 10 min and guanosine-5′-triphosphate (GTP, 0.4 mM final concentration) was added. The absorbance at 350 nm was immediately followed in a spectrophotometer. Baselines were established and temperature was quickly raised to 37 °C. At high concentrations compound **7** partially inhibits tubulin polymerization in an apparent concentration-dependent manner.

Fluorescence micrographs of nuclei (blue), tubulin (green) and phosphohistone H3 (red) staining demonstrated that vehicle-treated cells have highly organized microtubules and a low percentage of mitotic cells, while nanomolar concentrations of colchicine induced cellular microtubule disorganization and mitotic arrest (Fig. 9A and B). Cells treated with low micromolar cytotoxic concentrations of **7** had a phenotype of generally disorganized microtubules with seemingly lower overall tubulin content. Moreover, the general cellular structure was lost (Fig. 9C). Hoechst 33342 staining revealed the presence of condensed and fragmented nuclei characteristic of apoptosis (Fig. 9B and C). However, in contrast to colchicine, which caused an increased number of phosphohistone H3-positive cells, the same phenotype was not observed with **7**, suggesting that **7** did not arrest cells in mitosis.

The multi-parametric mitotic arrest assay also showed that both colchicine and **7** caused cell loss, either through detachment or lysis. Although we had previously demonstrated that **7** inhibited cell growth of different cancer cell lines at nanomolar doses, higher doses (in the micromolar range) were required to inhibit attachment and survival of HeLa cells (Table 7).[25] The EC_{50} values were obtained from the dose-response cell density curves. The form of the chromatin condensation, microtubule density and mitotic index graphs precluded IC_{50} determinations. Accordingly, we determined

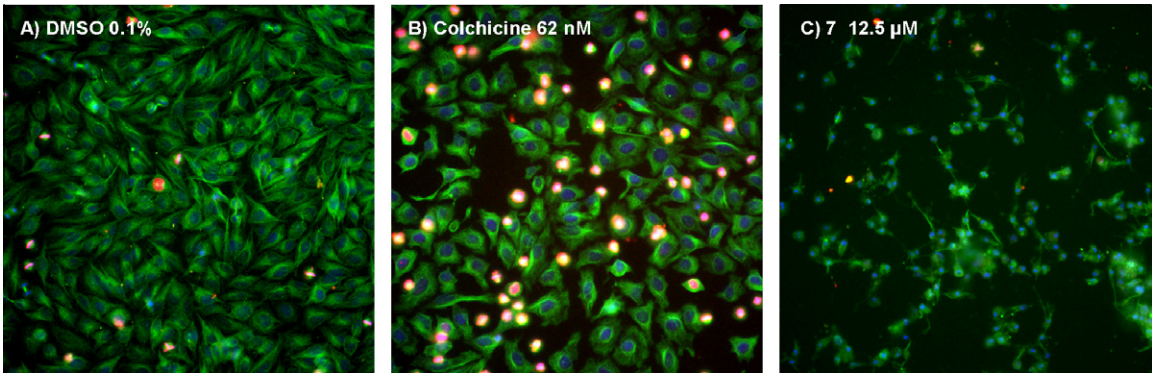

Figure 9. Immunofluorescence staining for markers of mitotic arrest in HeLa cells. HeLa cells were treated with (a) vehicle (DMSO 0.1%), (b) colchicine (62 nM) or (c) **7** (12.5 μM), followed by simultaneous immunostaining of α-tubulin (green), phosphohistone H3 (red), and Hoechst 33342 (blue). Vehicle-treated cells have highly organized microtubules and a low percentage of mitotic cells. Colchicine and **7** caused a heterogeneous response of tubulin disorganization, chromatin condensation, and nuclear fragmentation. Typical apoptotic morphology is observed for **7**. Images are representative fields from a single experiment repeated three times with similar results. Magnification: 200×.

Please cite this article in press as: Soares, M. A.; et al. *Bioorg. Med. Chem.* (2012), http://dx.doi.org/10.1016/j.bmc.2012.04.027

Table 7
Results of high-content analysis of mitotic arrest in HeLa cells[a]

Compound	EC_{50} (μM) cell density	MDEC (μM)[b]		
		Nuclear condensation	Tubulin intensity	Mitotic índex[c]
Colchicine	0.03	0.01	0.01	0.02
7	9.2 ± 0.8	5.8 ± 2.0	3.6 ± 0.1	> 50

[a] Average ± SD of four independent experiments, performed in quadruplicate.
[b] Minimum detectable effective concentration.
[c] Percentage of phosphohistone H3-positive cells.

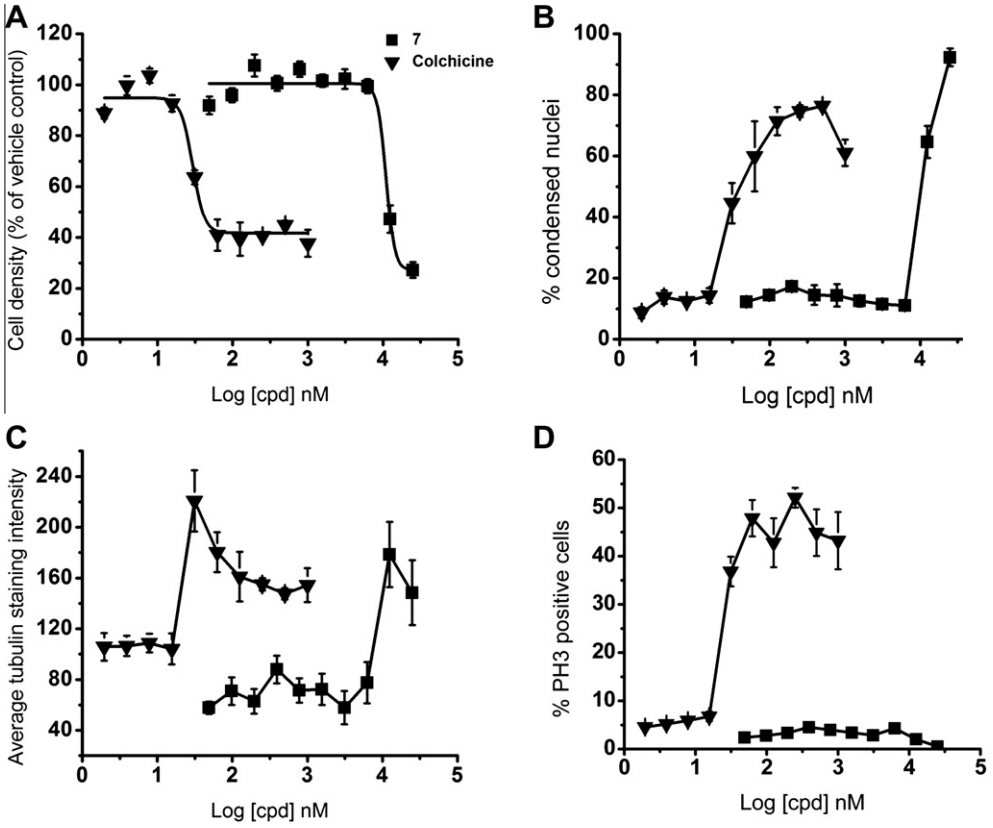

Figure 10. High-content analysis of mitotic arrest profiles in cells treated with the compounds being investigated. Cells were treated in 384-well plates with 10 twofold dilutions of either colchicine and **7** and analyzed by high-content analysis for (A) cell density, (B) chromatin condensation, (C) microtubule density and (D) mitotic index. All agents caused cell loss, enhanced nuclear condensation and induced cellular microtubule perturbations. Colchicine increased mitotic index, but this effect was not observed for **7**.

the minimum detectable effective concentration (MDEC) as an alternative measurement of **7** and colchicine activities.[37]

Cells treated with colchicine and **7** showed chromatin condensation and microtubule alterations (Fig. 10B, C and Table 7). Colchicine also provoked a concentration-dependent increase in the percentage of cells with elevated phosphohistone H3 levels, whereas **7** did not (Fig. 10D and Table 7). Therefore, despite its ability to partially inhibit tubulin assembly at high concentrations and to provoke cellular microtubule disorganization, **7** does not appear to cause mitotic arrest. As a consequence, direct interaction with tubulin is probably not responsible for the cytotoxic and pro-apoptotic effects of this compound.

3. Conclusion

Compound **1** and its N^4-*ortho* -*meta*- and -*para*-phenyl substituted derivatives presented cytotoxicity in nanomolar doses against malignant MCF-7 breast tumor cells and against U87 and T98G glioma cells, with good therapeutic index, as shown by their reduced haemolytic activity. In general, among the N^4-phenyl substituted derivatives, the *ortho* derivatives proved to be more cytotoxic than their *meta*- and *para* congeners.

Our results suggest that the studied thiosemicarbazones were able to induce programmed cell death in tumor cells. The results described thus far suggest that these compounds induce both apoptosis and autophagy in the studied malignant tumor cells.

Despite their abilities to partially inhibit tubulin assembly at high concentrations and to provoke cellular microtubule disorganization, the thiosemicarbazones did not behave as mitotic arresters. As a consequence, direct interaction with tubulin is probably not primarily responsible for their cytotoxic and pro-apoptotic effects. The high cytotoxic activity of the studied compounds, together with their good therapeutic index, indicates that they are promising as antitumor drug candidates for the treatment of breast tumors and malignant gliomas.

Please cite this article in press as: Soares, M. A.; et al. *Bioorg. Med. Chem.* (2012), http://dx.doi.org/10.1016/j.bmc.2012.04.027

4. Material and methods

4.1. Chemicals

2-Acetylpyridine, hydrazine dihydrate, *o*-fluorophenyl-, *m*-fluorophenyl-, *p*-fluorophenyl-, *o*-chlorophenyl-, *m*-chlorophenyl-, *p*-chlorophenyl-, *o*-iodophenyl-, *m*-iodophenyl-, *p*-iodophenyl-, *o*-nitrophenyl-, *m*-nitrophenyl- and *p*-nitrophenyl-isothiocyanate were purchased from Aldrich or Alfa Aesar and were used as received. **1** and its fluoro (**2–4**), chloro (**5–7**) and nitro (**11–13**) derivatives were prepared as previously described.[29]

4.2. Physical measurements

Infrared spectra were recorded on a Perkin Elmer FT-IR Spectrum GX spectrometer using KBr plates (4000–400 cm^{-1}). NMR spectra were obtained at room temperature with a Brucker DRX-400 Avance (400 MHz) spectrometer using DMSO-d_6 as the solvent and tetramethylsilane (TMS) as internal reference. Melting Points were determined on a Mettler FP 90 equipment. Compound's purities were established by HPLC (HPLC Agilent Technologies 1200) with an UV detector at 314 nm, using Supelcosil C18 column (5 μm particle size, 25 cm × 4.6 mm) and eluting with methanol. HPLC data indicated purity >98% for all compounds except for compounds **6** and **7** (purities = 97 and 94%, respectively). High resolution MS measurements were performed on a Shimadzu LCMS-IT-TOF mass spectrometer.

4.3. Synthesis of 2-acetylpyridine N^4-*ortho*-(8), N^4-*meta*- (9) and N^4-*para*-iodophenyl (10) thiosemicarbazones

Hidrazine dihydrate (39 mmol, 30% of excess) was added to 2-acetylpyridine (30 mmol) in methanol under stirring at room temperature. After 24 h, the product 2-acetylpyridine hydrazone was filtered off. The thiosemicarbazones were prepared by stirring 2-acetylpyridine hydrazone with *o*-, *m*- or *p*-iodophenyl isothiocyanate in 1:1 molar ratio under reflux in ethanol for 6 h. The solids were filtered off, washed with ethanol followed by diethyl ether, and dried in vacuo.

4.3.1. 2-Acetylpyridine N^4-*ortho*-iodo-phenyl thiosemicarbazone (8)

White powder. Yield: 70%; Melting point: 173.0–173.9 °C; IR (KBr,cm^{-1}): 3306, 3208 (*ν* (NH)), 1582 (*ν*(C=N)), 782 (*ν*(C=S)), 621 (ρ(py)); ^{1}H NMR (200 MHz, DMSO-d_6): *δ* (ppm, *E* isomer (95%)) = 10.90 (s, 1H, N^3-H), 10.14 (s, 1H, N^4-H), 8.61 (d, *J* = 6.06 Hz, 1H, H6), 8.57 (d, 1H, *J* = 8.35 Hz, H3), 7.82 (t, 1H, *J* = 7.99 Hz, H4), 7.55–7.35 (m, 1H, H5), 2.49 (s, 3H, H15); *δ* (ppm, *Z* isomer (5%)) = 14.66 (s, 1H, N^3-H), 10.21 (s, 1H, N^4-H), 8.81 (d, *J* = 5.59 Hz, 1H, H6), 8.11 (t, *J* = 8.00 Hz, 1H, H4); ^{13}C NMR (200 MHz, DMSO-d_6): *δ* (ppm, *E* isomer (95%)) 177.43 (C8), 154.42 (C2), 148.39 (C6), 141.07 (C7), 136.33 (C4), 121.07 (C3), 148.87 (C9), 124.01 (C5), 12.44 (C15); HRMS *m*/*z* $[M-H]^-$ calcd for $C_{14}H_{12}N_4SI$: 394.9833, found: 394.9837.

4.3.2. 2-Acetylpyridine N^4-*meta*-iodo-phenyl thiosemicarbazone (9)

Yellow powder. Yield: 94%; Melting point: 175.9–177.9 °C; IR (KBr, cm^{-1}): 3264 (*ν*(NH)), 1595 (*ν*(C=N)), 786 (*ν*(C=S)), 616 ((py)); ^{1}H NMR (200 MHz, DMSO-d_6): *δ* (ppm, *E* isomer (87%)) = 10.83 (s, 1H, N^3-H), 10.22 (s, 1H, N^4-H), 8.62 (d, *J* = 4.68 Hz, 1H, H6), 8.55 (d, 1H, *J* = 8.04 Hz, H3), 7.84 (t, 1H, *J* = 7.64 Hz, H4), 7.42 (t, 1H, *J* = 5.32 Hz, H5), 2.49 (s, 3H, H15); *δ* (ppm, *Z* isomer (13%)) = 14.69 (s, 1H, N^3-H), 10.37 (s, 1H, N^4-H), 8.80 (d, *J* = 4.24 Hz, 1H, H6); ^{13}C NMR (200 MHz, DMSO-d_6): *δ* (ppm, *E* isomer (87%)) 177.01 (C8), 154.32 (C2), 148.39 (C6), 140.43 (C7), 136.28 (C4), 121.21 (C3), 149.54 (C9), 124.08 (C5), 12.55 (C15); HRMS *m*/*z* $[M-H]^-$ calcd for $C_{14}H_{12}N_4SI$: 394.9833, found: 394.9835.

4.3.3. 2-Acetylpyridine N^4-*para*-iodo-phenyl thiosemicarbazone (10)

Light yellow powder. Yield: 89%; Melting point: 205.0–206.1 °C; IR (KBr, cm^{-1}): 3294, 3232 (*ν*(NH)), 1581 (*ν*(C=N)), 783 (*ν*(C=S)), 621 ((py)); ^{1}H NMR (200 MHz, DMSO-d_6): *δ* (ppm, *E* isomer (94%)) = 10.79 (s, 1H, N^3-H), 10.19 (s, 1H, N^4-H), 8.60 (d, *J* = 4.39 Hz, 1H, H6), 8.52 (d, 1H, *J* = 8.04 Hz, H3), 7.82 (t, 1H, *J* = 7.83 Hz, H4), 7.50-7.53 (m, 1H, H5), 2.47 (s, 3H, H15); *δ* (ppm, *Z* isomer (6%)) = 14.66 (s, 1H, N^3-H), 10.33 (s, 1H, N^4-H), 8.79 (d, *J* = 4.12 Hz, 1H, H6), 8.10 (t, *J* = 7.79 Hz, 1H, H4); ^{13}C NMR (200 MHz, DMSO-d_6): *δ* (*E* isomer (94%)) 176.98 (C8), 154.34 (C2), 148.41 (C6), 149.51 (C7), 136.70 (C4), 121.19 (C3), 138.93 (C9), 124.07 (C5), 12.54 (C15); HRMS *m*/*z* $[M-H]^-$ calcd for $C_{14}H_{12}N_4SI$: 394.9833, found: 394.9837.

4.4. Crystal structures determination

The crystal structures of **2–4**, **8**, **10** and **11** were determined by using single-crystal X-ray diffractometry. The measurements were carried out on an Oxford-Diffraction GEMINI-Ultra diffractometer using graphite-Enhance Source Mo K_α radiation (*λ* = 0.71073 Å) at 293(2) K. The data collection, cell refinements, and data reduction were performed using the CRYSALISPRO software.[39] Semi-empirical from equivalents absorption correction method was applied.[39]

The structures were solved by direct methods using SHELXS-97.[40] Full-matrix least-squares refinement procedure on F^2 with anisotropic thermal parameters was carried on using SHELXL-97.[40] Positional and anisotropic atomic displacement parameters were refined for all non-hydrogen atoms. Hydrogen atoms were placed geometrically and the positional parameters were refined using a riding model. Hydrogen atoms were placed geometrically and the positional parameters were refined using a riding model.

Molecular graphics and packing figures were plotted using ORTEP[41] and PLATON,[42] respectively.

4.5. Cell lines and culture conditions

Malignant human tumor cell lines MCF-7, U87 and T98G were obtained from the American Type Culture Collection (ATCC, USA) and maintained in Dulbeccós Modified Eagle's Medium (DMEM, Gibco), supplemented with 10% foetal bovine serum (Cultilab) and antibiotics (50 U mL^{-1} penicillin/50 μM streptomycin), in a humidified atmosphere air/CO_2 (5%/95%) at 37 °C. For all experiments, cells were seeded in 96-well plates, at a density of 1–2 × 10^3 cells/well.

4.6. Cytotoxic activity

Cytotoxicity was evaluated by the 3-(4,5-dimethyl-2-thiazolyl)-2,5-diphenyl-2*H*-tetrazolium bromide (MTT) assay which measures the cellular metabolic viability.[43] The cells were cultured in 96-well plates and, 12 h after incubation, they were treated with different concentrations of test compounds (1 × 10^{-12} M^{-1} × 10^{-5} M). Another group of cells was treated with the same concentrations of etoposide (positive control), an antineoplasic agent that inhibits the enzyme topoisomerase II. Compounds were previously dissolved in DMSO and the final concentrations were adjusted, through an 8-fold serial dilution, in DMEM in such manner that the final DMSO concentration was lower than 0.5%.

After 48 h-treatment the cells were incubated with MTT (0.5 mg mL^{-1}), and formazan crystals were solubilised in DMSO.

Absorbance was measured in a microplate reader at 570 nm. Tests using DMSO (0.5% in DMEM) as negative control were carried out in parallel. IC_{50} values were calculated as the concentration of compound that induced 50% of cytotoxicity. Data were presented as average ± standard deviation. All experiments were carried out in quadruplicates and repeated in at least three independent experiments with full agreement between the results. The statistical significance was assessed using Student's *t*-test (p <0.05).

4.7. SAR studies

Conformational analysis of thiosemicarbazones was performed using the Merck Molecular Force Field (MMFF)[44] implemented in the Tinker Molecular Modeling Program.[45] For all compounds the *E* and *Z* isomers were analyzed. The minimum energy structures of the isomers obtained in the conformational analysis step were further optimized at the Density Functional Theory[46] level, employing the hybrid B3LYP[47,48] exchange-correlation functional and using the cc-pVDZ[49] all electron basis set[50,51] for all atoms. In order to have better properties and energetic results, single point energy calculations at the second order Møller-Plesset perturbation theory level[52,53] were then performed on the optimized B3LYP/cc-pVDZ structures, using the same basis set (MP2/cc-pVDZ//B3LYP/cc-pVDZ). The inner shell electrons of iodine were treated by the effective core potential LANL2DZ[54] and its associated double-ζ basis set was used for the valence electrons (5s,5p). The charge distribution on the most stable conformers was computed using the Natural Bonding Orbital (NBO) formalism.[55,56] All quantum mechanical calculations were performed using the Gaussian program.[57] HOMO and LUMO energies, dipole, NBO charges of sulfur and nitrogen from pyridine (N_{pyr}) and azomethine group (N_{azo}) were obtained after full optimization and were used as descriptors for further SAR studies. Superficial molecular area and logP were also used as descriptors for SAR studies. The three-dimensional structures obtained from optimization of thiosemicarbazones were used as input in the Marvin software[58] to calculate the superficial molecular area. Calculations of log*P* for the thiosemicarbazones were performed using ALOGPS 2.1 software, accessed via the Virtual Computational Chemistry Laboratory interface.[59]

4.8. Morphological analysis of tumor cells

Cells were plated in 96-well plates and treated with test compounds **1–13** (1 μM). Morphological changes were analyzed 48 h after the treatment by contrast-phase microscopy (Nikon).

DNA alterations were detected by DAPI staining. After 48 h-treatment with 1 μM of test compounds, cells were washed with phosphate buffered saline (PBS) and fixed with 70% methanol at room temperature for 30 min. Cells were incubated with 0.4 μg mL^{-1} DAPI (Sigma) for 1 h in the dark after washing with PBS. DNA alterations such as condensation and fragmentation were observed by fluorescence microscopy (Nikon – 385–410 nm).

4.9. Acridine orange-ethidium bromide (AO/EB) doubling staining assay

Acridine orange, a cationic dye, has been the subject of extensive studies in recent years because of its metachromatic staining properties and can be used in conjunction with ethidium bromide to differentiate among alive, apoptotic, necrotic and autophagic cells.[60]

Acridine orange/ethidium bromide doubling staining was performed according to Baskic et al.[34] with modifications. MCF-7, U87 and T98G cells were seeded in 96-well plates and treated with test compounds **1–13** (1 μM) for 48 h. After treatment, cells were incubated with serum-free medium, containing 1 μg mL^{-1} acridine orange (Sigma) and 1 μg mL^{-1} ethidium bromide (Sigma), for 15 min. The medium was removed and fluorescent micrographs were obtained using an inverted fluorescence microscope (Nikon – 530–650 nm). Viable cells presented uniform bright green nuclei; early apoptotic cells (which still have intact membranes and did not stain with ethidium bromide) have green nuclei, but chromatin condensation is visible as bright green fragments; late apoptotic cells have orange to red nuclei with condensed or fragmented chromatin and necrotic cells have uniformly orange to red nuclei.

4.10. Direct haemolysis assay

The haemolytic activity of thiossemicarbazones was evaluated according to Fisher et al.[61] Human blood, collected in tubes containing EDTA, was centrifuged at 700x*g* for 10 min. The pellet was washed tree times with cold PBS pH 7.4 by centrifugation, and re-suspended in the same buffer. Thiossemicarbazones' solutions of different concentrations were added to the erythrocytes and were incubated for 1 h at 37 °C in a shaker water bath. The release of haemoglobin was determined after centrifugation by photometric analyses at 540 nm. Complete haemolysis was achieved using 5% Triton X-100 yielding the 100% control value.

4.11. Inhibition of tubulin assembly

Since all studied thiosemicarbazones induced cellular phenotypic changes characteristics of apoptosis in a similar way, the inhibition of tubulin assembly and microtubule stabilization assays were only performed for H2Ac4*p*ClPh (**7**), one of the most cytotoxic compounds.

Electrophoretically homogeneous bovine brain tubulin (final concentration 10 μM; 1 mg mL^{-1}) was pre-incubated with test agents (colchicine and compound **7**) dissolved in DMSO (1% v/v final concentration) and monosodium glutamate (0.8 M final concentration) at 30 °C in 96-well plates. The reaction mixtures were cooled to 0 °C for 10 min and GTP (0.4 mM final concentration) was added. The absorbance at 350 nm was immediately followed in a spectrophotometer. Baselines were established and temperature was quickly raised to 37 °C. The turbidity value after 20 min at 30 °C for DMSO 1% was assigned as 100% assembly, and for colchicine 2.5 μM as 0% assembly. To observe concentration-dependent effects of the tested compounds, four twofold dilutions of them were evaluated.

4.12. Automated high-content cellular analyses

The effects of colchicine and **7** on mitotic arrest, nuclear morphology and cellular microtubules were studied as previously described.[37,38] HeLa human cervical carcinoma cells (8000/well) were plated in collagen-coated 384-well microplates and treated in quadruplicate with vehicle (DMSO 0.1% final concentration) or 10 twofold dilutions of test compounds within 4–6 h of seeding. Cells were incubated for 18 h at 37 °C and CO_2 5%, fixed with formaldehyde, and labeled with 10 μg mL^{-1} Hoechst 33342 in Hank's balanced salt solution (HBSS). Cells were permeabilized with 0.5% (w/w) Triton-X100 for 5 min at room temperature and incubated with a primary antibody cocktail consisting of an HBSS solution containing rabbit polyclonal antiphosphohistone H3 (Ser10, 1:500, Upstate, Charlottesville, VA, USA), and mouse monoclonal anti-α-tubulin (1:3000, Sigma, St. Louis, MO, USA), followed by a mixture of FITC-labeled donkey anti-mouse IgG (1:500) and Cy3-labeled donkey anti-rabbit IgG (1:500) as secondary cocktail. Cells were rinsed once with HBSS and stored at 4 °C in HBSS until analysis. Microplates were analyzed with an ArrayScanII instrument (Cellomics, Pittsburgh, PA, USA) using the Target Activation Bioapplication

(Cellomics, Inc.,). Within the application, 1000 individual cells in each well were imaged at three different wavelengths using an Omega XF93 filter set (Omega Optical, Inc., Brattleboro, VT, USA) at excitation/emission wavelengths of 350/461 nm (Hoechst), 494/519 nm (FITC), and 556/573 nm (Cy3). The following parameters were used for data analysis: average nuclear intensity, nuclei per field, average nuclear FITC intensity, and average nuclear Cy3 intensity. A nuclear mask was generated from Hoechst 33342-stained nuclei. Microtubule density and histone H3 phosphorylation were measured in the FITC and Cy3 channel, respectively. Microtubule density was defined as the average green (FITC) pixel intensity in an area defined by the nuclear mask. For determination of mitotic index and nuclear condensation, thresholds for Hoechst 33342 and phosphohistone-H3 intensities were defined as the average Hoechst 33342 or Cy3 intensity plus 1 SD from 28 vehicle-treated wells placed in the center of the microplate. Cells were classified as positive if their average Hoechst 33342 or Cy3 intensity exceeded this threshold. To visually illustrate the effects of test agents on cellular microtubules and mitotic arrest, the identical 384-well plates were then used to acquire higher resolution images of selected wells.

Acknowledgements

This work was supported by CNPq (Conselho Nacional de Desenvolvimento Científico e Tecnológico), CNEN (Comissão Nacional de Energia Nuclear), FAPEMIG (Fundação de Amparo à Pesquisa do Estado de Minas Gerais), INCT-INOFAR (Instituto Nacional de Ciência e Tecnologia de Fármacos e Medicamentos, Proc. CNPq 573.364/2008-6), INCT-MM (Instituto Nacional de Ciência e Tecnologia de Medicina Molecular, Proc. FAPEMIG: CBB-APQ-00075-09/CNPq 573646/2008-2), INCT-Catálise (Instituto Nacional de Ciência e Tecnologia de Catálise em Sistemas Moleculares e Nanoestruturados) and FAPESP (Fundação de Amparo à Pesquisa do Estado de São Paulo). The authors express sincere thanks to LabCRI (UFMG), particularly to Professor Nilvado L. Speziali for the X-ray facilities and measurements.

Supplementary data

Supplementary data associated with this article can be found, in the online version, at http://dx.doi.org/10.1016/j.bmc.2012.04.027.

References and notes

1. 'WHO—World Health Organization", http://www.who.int/cancer (Accessed June 2011).
2. Coughlin, S. S.; Ekwueme, D. U. *Cancer Epidemiol.* **2009**, *33*, 315.
3. Wardley, A. *Breast* **2008**, *17*, 285.
4. Louis, D. N.; Pomeroy, S. L.; Cairncross, J. G. *Cancer Cell.* **2002**, *1*, 125.
5. Louis, D. N.; Ohgaki, H.; Wiestler, O. D.; Cavenee, W. K.; Burger, P. C.; Jouvet, A.; Scheithauer, B. W.; Kleihues, P. *Acta Neuropathol.* **2007**, *114*, 97.
6. Stupp, R.; Mason, W. P.; van den Bent, M. J.; Weller, M.; Fisher, B.; Taphoorn, M. J.; Belanger, K.; Brandes, A. A.; Marosi, C.; Bogdahn, U.; Curschmann, J.; Janzer, R. C.; Ludwin, S. K.; Gorlia, T.; Allgeier, A.; Lacombe, D.; Cairncross, J. G.; Eisenhauer, E.; Mirimanoff, R. O. N. *Engl. J. Med.* **2005**, *352*, 987.
7. van den Bent, M.; Chinot, O.; Cairncross, J. G. *Neuro-Oncol.* **2003**, 128.
8. Parsons, D. W.; Jones, S.; Zhang, X.; Lin, J. C.; Leary, R. J.; Angenendt, P.; Mankoo, P.; Carter, H.; Siu, I.; Gallia, G. L.; Olivi, A.; McLendon, R.; Rasheed, B. A.; Keir, S.; Nikolskaya, T.; Nikolsky, Y.; Busam, D. A.; Tekleab, H.; Diaz, L. A., Jr; Hartigan, J.; Smith, D. R.; Strausberg, R. L.; Marie, S. K. N.; Shinjo, S. M. O.; Yan, H.; Riggins, G. J.; Bigner, D. D.; Karchin, R.; Papadopoulos, N.; Parmigiani, G.; Vogelstein, B.; Velculescu, V. E.; Kinzler, K. W. *Science* **1807**, *2008*, 321.
9. Colli, B. O.; Carlotti, C. G., Jr *J. Bras. Neurocir.* **2001**, *12*, 36.
10. Beraldo, H.; Gambino, D. *Mini-Rev. Med. Chem.* **2004**, *4*, 31.
11. Finch, R. A.; Liu, M.; Grill, S. P.; Rose, W. C.; Loomis, R.; Vasquez, K. M.; Cheng, Y.; Sartorelli, A. C. *Biochem. Pharmacol.* **2000**, *59*, 983.
12. Finch, R. A.; Liu, M.; Cory, A. H.; Cory, J. G.; Sartorelli, A. C. *Advan. Enzyme Regul.* **1999**, *39*, 3.
13. Gojo, I.; Tidwell, M. L.; Greer, J.; Takebe, N.; Seiter, K.; Pochron, M. F.; Johnson, B.; Sznol, M.; Karp, J. E. *Leuk. Res.* **2007**, *31*, 1165.
14. Shao, J.; Zhou, B.; Chu, B.; Yen, Y. *Cancer Drug Targets* **2006**, *6*, 409.
15. Quiroga, A. G.; Pérez, J. M.; Montero, E. I.; Masaguer, J. R.; Alonso, C.; Navarro-Ranninger, C. J. *J. Inorg. Biochem.* **1998**, *70*, 117.
16. Quiroga, A. G.; Navarro-Ranninger, C. *Coord. Chem. Rev.* **2004**, *248*, 119.
17. Bal, T.; Atasever, B.; Solakoğlu, Z.; Erdem-Kuruca, S.; Ülküseven, B. *Eur. J. Med. Chem.* **2007**, *42*, 161.
18. Ferrari, M. B.; Bisceglie, F.; Pelosi, G.; Tarasconi, P.; Albertini, R.; Bonati, A.; Lunghi, P.; Pinelli, S. *J. Inorg. Biochem.* **2001**, *83*, 169.
19. Li, M. X.; Chen, C. L.; Ling, C. S.; Zhou, J.; Ji, B. S.; Wu, Y. J.; Niu, J. Y. *Bioorg. Med. Chem. Lett.* **2009**, *19*, 2704.
20. Ferraz, K. S. O.; Ferandes, L.; Carrilho, D.; Pinto, M. C. X.; Leite, M. F.; Souza-Fagundes, E. M.; Speziali, N. L.; Mendes, I. C.; Beraldo, H. *Bioorg. Med. Chem.* **2009**, *17*, 7138.
21. Rebolledo, A. P.; Vieites, M.; Gambino, D.; Piro, O. E.; Castellano, E. E.; Zani, C. L.; Souza-Fagundes, E. M.; Teixeira, L. R.; Batista, A. A.; Beraldo, H. *J. Inorg. Biochem.* **2005**, *99*, 698.
22. Lessa, J. A.; Guerra, J. C.; Miranda, L. F.; Romeiro, C. F. D.; Da Silva, J. G.; Mendes, I. M.; Speziali, N. L.; Souza-Fagundes, E. M.; Beraldo, H. *J. Inorg. Biochem.* **2011**, *105*, 1729.
23. Rebolledo, A. P.; Ayala, J. D.; Lima, G. M.; Marchini, N.; Bombieri, G.; Zani, C. L.; Souza-Fagundes, E. M.; Beraldo, H. *Eur. J. Med. Chem.* **2005**, *40*, 467.
24. Reis, D. C.; Pinto, M. C. X.; Souza-Fagundes, E. M.; Wardell, S. M. S. V.; Wardell, J. L.; Beraldo, H. *Eur. J. Med. Chem.* **2010**, *45*, 3904.
25. Lessa, J. A.; Mendes, I. C.; da Silva, P. R. O.; Soares, M. A.; dos Santos, R. G.; Speziali, N. L.; Romeiro, N. C.; Barreiro, E. J.; Beraldo, H. *Eur. J. Med. Chem.* **2010**, *45*, 5671.
26. Kondo, Y.; Kondo, S. *Autophagy* **2006**, *2*, 85.
27. Akar, U.; Chaves-Reyez, A.; Barria, M.; Tari, A.; Sanguino, A.; Kondo, Y.; Kondo, S.; Arun, B.; Lopez-Berestein, G.; Ozpolat, B. *Autophagy* **2008**, *4*, 669.
28. Høyer-Hansen, M.; Jäättelä, M. *Autophagy* **2008**, *4*, 574.
29. Klayman, D. L.; Bartosevich, J. F.; Griffin, T. S.; Mason, C. J.; Scovill, J. P. *J. Med. Chem.* **1979**, *22*, 855.
30. Bermejo, E.; Castiñeiras, A.; Dominguez, R.; Carballo, R.; Maichle-Moessmer, C.; Straehle, J.; West, D. X. *Anorg. Allg. Chem.* **1999**, *625*, 961.
31. Ribble, D.; Goldstein, N. B.; Norris, D. A.; Shellman, Y. G. *BMC Biotechnol.* **2005**, *12*, 1.
32. Yang, C.; Kaushal, V.; Shah, S. V.; Kaushal1, P. G. *Am. J. Physiol. Renal Physiol.* **2008**, *294*, 777.
33. Klionsky, D. J.; Abeliovich, H.; Agostinis, P.; Agrawal, D. K.; Aliev, G.; Askew, D. S.; Baba, M.; Baehrecke, E. H.; Bahr, B. A.; Ballabio, A.; Bamber, B. A.; Bassham, D. C.; Bergamini, E.; Bi, X.; Biard-Piechaczyk, M.; Blum, J. S.; Bredesen, D. E.; Brodsky, J. L.; Brumell, J. H.; Brunk, U. T.; Bursch, W.; Camougrand, N.; Cebollero, E.; Cecconi, F.; Chen, Y.; Chin, L. S.; Choi, A.; Chu, C. T.; Chung, J.; Clarke, P. G.; Clark, R. S.; Clarke, S. G.; Clavé, C.; Cleveland, J. L.; Codogno, P.; Colombo, M. I. I.; Coto-Montes, A.; Cregg, J. M.; Cuervo, A. M.; Debnath, J.; Demarchi, F.; Dennis, P. B.; Dennis, P. A.; Deretic, V.; Devenish, R. J.; Di Sano, F.; Dice, J. F.; Difiglia, M.; Dinesh-Kumar, S.; Distelhorst, C. W.; Djavaheri-Mergny, M.; Dorsey, F. C.; Dröge, W.; Dron, M.; Dunn, W. A., Jr.; Duszenko, M.; Eissa, N. T.; Elazar, Z.; Esclatine, A.; Eskelinen, E. L.; Fésüs, L.; Finley, K. D.; Fuentes, J. M.; Fueyo, J.; Fujisaki, K.; Galliot, B.; Gao, F. B.; Gewirtz, D. A.; Gibson, S. B.; Gohla, A.; Goldberg, A. L.; Gonzalez, R.; González-Estévez, C.; Gorski, S.; Gottlieb, R. A.; Häussinger, D.; He, Y. W.; Heidenreich, K.; Hill, J. A.; Høyer-Hansen, M.; Hu, X.; Huang, W. P.; Iwasaki, A.; Jäättelä, M.; Jackson, W. T.; Jiang, X.; Jin, S.; Johansen, T.; Jung, J. U.; Kadowaki, M.; Kang, C.; Kelekar, A.; Kessel, D. H.; Kiel, J. A.; Kim, H. P.; Kimchi, A.; Kinsella, T. J.; Kiselyov, K.; Kitamoto, K.; Knecht, E.; Komatsu, M.; Kominami, E.; Kondo, S.; Kovács, A. L.; Kroemer, G.; Kuan, C. Y.; Kumar, R.; Kundu, M.; Landry, J.; Laporte, M.; Le, W.; Lei, H. Y.; Lenardo, M. J.; Levine, B.; Lieberman, A.; Lim, K. L.; Lin, F. C.; Liou, W.; Liu, L. F.; Lopez-Berestein, G.; López-Otín, C.; Lu, B.; Macleod, K. F.; Malorni, W.; Martinet, W.; Matsuoka, K.; Mautner, J.; Meijer, A. J.; Meléndez, A.; Michels, P.; Miotto, G.; Mistiaen, W. P.; Mizushima, N.; Mograbi, B.; Monastyrska, I.; Moore, M. N.; Moreira, P. I.; Moriyasu, Y.; Motyl, T.; Münz, C.; Murphy, L. O.; Naqvi, N. I.; Neufeld, T. P.; Nishino, I.; Nixon, R. A.; Noda, T.; Nürnberg, B.; Ogawa, M.; Oleinick, N. L.; Olsen, L. J.; Ozpolat, B.; Paglin, S.; Palmer, G. E.; Papassideri, I.; Parkes, M.; Perlmutter, D. H.; Perry, G.; Piacentini, M.; Pinkas-Kramarski, R.; Prescott, M.; Proikas-Cezanne, T.; Raben, N.; Rami, A.; Reggiori, F.; Rohrer, B.; Rubinsztein, D. C.; Ryan, K. M.; Sadoshima, J.; Sakagami, H.; Sakai, Y.; Sandri, M.; Sasakawa, C.; Sass, M.; Schneider, C.; Seglen, P. O.; Seleverstov, O.; Settleman, J.; Shacka, J. J.; Shapiro, I. M.; Sibirny, A.; Silva-Zacarin, E. C.; Simon, H. U.; Simone, C.; Simonsen, A.; Smith, M. A.; Spanel-Borowski, K.; Srinivas, V.; Steeves, M.; Stenmark, H.; Stromhaug, P. E.; Subauste, C. S.; Sugimoto, S.; Sulzer, D.; Suzuki, T.; Swanson, M. S.; Tabas, I.; Takeshita, F.; Talbot, N. J.; Tallóczy, Z.; Tanaka, K.; Tanaka, K.; Tanida, I.; Taylor, G. S.; Taylor, J. P.; Terman, A.; Tettamanti, G.; Thompson, C. B.; Thumm, M.; Tolkovsky, A. M.; Tooze, S. A.; Truant, R.; Tumanovska, L. V.; Uchiyama, Y.; Ueno, T.; Uzcátegui, N. L.; Van der Klei, I.; Vaquero, E. C.; Vellai, T.; Vogel, M. W.; Wang, H. G.; Webster, P.; Wiley, J. W.; Xi, Z.; Xiao, G.; Yahalom, J.; Yang, J. M.; Yap, G.; Yin, X. M.; Yoshimori, T.; Yu, L.; Yue, Z.; Yuzaki, M.; Zabirnyk, O.; Zheng, X.; Zhu, X.; Deter, R. L. *Autophagy* **2008**, *4*, 151.
34. Baskic, D.; Popovi, S.; Ristic, P.; Nebojsa, N.; Arsenijevic, N. *Cell. Biol. Internat.* **2006**, *30*, 924.
35. Lee, S. B.; Tong, S. Y.; Kim, J. J.; Um, S. J.; Park, J. S. *DNA Cell Biol.* **2007**, *26*, 713.
36. Jordan, M. A. *Curr. Med. Chem. Anticancer Agents* **2002**, *2*, 1.
37. Wang, Z.; McPherson, P. A.; Raccor, B. S.; Balachandran, R.; Zhu, G.; Day, B. W.; Vogt, A.; Wipf, P. *Chem. Biol. Drug Des.* **2007**, *70*, 75.
38. Vogt, A.; McPherson, P. A.; Shen, X.; Balachandran, R.; Zhu, G.; Raccor, B. S.; Nelson, S. G.; Tsang, M.; Day, B. W. *Chem. Biol. Drug Des.* **2009**, *74*, 358.

39. CRYSALISPRO, Oxford Diffraction Ltd., Version 1.171.34.34 (release 05–01-2010 CrysAlis171.NET.
40. Sheldrick, G. M. SHELXL-97: Program for Crystal Structures Analysis, University of Göttingen, Göttingen, Germany, 1997.
41. Farrugia, L. J. *J. Appl. Crystallogr.* **1997**, *30*, 565.
42. Spek, A. L. *Acta Cryst.* **2009**, *D65*, 148.
43. Plumb, J. A.; Miloroy, R.; Kaye, S. B. *Cancer Res.* **1989**, *49*, 4435.
44. Dewar, M. J. S.; Zoebisch, E. G.; Healy, E. F.; Stewart, J. J. P. *J. Am. Chem. Soc.* **1985**, *107*, 3902.
45. TINKER Software Tools for Molecular Design, 5.0. Jay W. Ponder Lab, Dept. of Biochemistry & Molecular Biophysics, Washington University School of Medicine: St. Louis, **2009**.
46. Parr, R. G.; Yang, W. *Density-Functional Theory of Atoms and Molecule*; Oxford University Press: Oxford, 1989.
47. Becke, A. D. *J. Chem. Phys.* **1993**, *98*, 5648–5652.
48. Lee, C.; Yang, W.; Parr, R. G. *Phys. Rev.* **1988**, *37*, 785.
49. Dunning, T. H., Jr *J. Chem. Phys.* **1989**, *90*, 1007.
50. Ditchfield, R.; Hehre, W. J.; Pople, J. A. *J. Chem. Phys.* **1971**, *54*, 724.
51. Hehre, W. J.; Ditchfield, R.; Pople, J. A. *J. Chem. Phys.* **1972**, *56*, 2257.
52. Møller, C.; Plesset, M. S. *Phys. Rev.* **1934**, *46*, 618.
53. Szabo, A.; Ostlund, N. S. *Modern Quantum Chemistry, Introduction to Advanced Electronic Structure Theory*; Dover Publication, Inc: New York, 1996.
54. Hay, P. J.; Wadt, W. R. *J. Chem. Phys.* **1985**, *82*, 284.
55. Reed, A. E.; Weinhold, F. *J. Chem. Phys.* **1983**, *78*, 4066.
56. Reed, A. E.; Weinstock, R. B.; Weinhold, F. *J. Chem. Phys.* **1985**, *83*, 735.
57. Frisch, M. J.; Trucks, G. W.; Schlegel, H. B.; Scuseria, G. E.; Robb, M. A.; Cheeseman, J. R.; Montgomery, Jr., J. A.; Vreven, T.; Kudin, K. N.; Burant, J. C.; Millam, J. M.; Iyengar, S. S.; Tomasi, J.; Barone, V.; Mennucci, B.; Cossi, M.; Scalmani, G.; Rega, N.; Petersson, G. A.; Nakatsuji, H.; Hada, M.; Ehara, M.; Toyota, K.; Fukuda, R.; Hasegawa, J.; Ishida, M.; Nakajima, T.; Honda, Y.; Kitao, O.; Nakai, H.; Klene, M.; Li, X.; Knox, J. E.; Hratchian, H. P.; Cross, J. B.; Bakken, V.; Adamo, C.; Jaramillo, J.; Gomperts, R.; Stratmann, R. E.; Yazyev, O.; Austin, A. J.; Cammi, R.; Pomelli, C.; Ochterski, J. W.; Ayala, P. Y.; Morokuma, K.; Voth, G. A.; Salvador, P.; Dannenberg, J. J.; Zakrzewski, V. G.; Dapprich, S.; Daniels, A. D.; Strain, M. C.; Farkas, O.; Malick, D. K.; Rabuck, A. D.; Raghavachari, K.; Foresman, J. B.; Ortiz, J. V.; Cui, Q.; Baboul, A. G.; Clifford, S.; Cioslowski, J.; Stefanov, B. B.; Liu, G.; Liashenko, A.; Piskorz, P.; Komaromi, I.; Martin, R. L.; Fox, D. J.; Keith, T.; Al-Laham, M. A.; Peng, C. Y.; Nanayakkara, A.; Challacombe, M.; Gill, P. M. W.; Johnson, B.; Chen, W.; Wong, M. W.; Gonzalez, C.; Pople, J. A.; Gaussian 03, Revision C.02, Gaussian, Inc., Wallingford CT, **2004**.
58. MarvinSketch 5.5.1.0 Program. ChemAxon, http://www.chemaxon.com/products.html.
59. ALOGPS 2.1 Program. Available: http://www.vcclab.org/lab/alogps (Accessed April 2011).
60. Beers, R. F. *J. Bacteriol.* **1964**, *88*, 1249.
61. Fisher, D.; Li, Y.; Ahlemeyer, B.; Krieglstein, J.; Kissel, T. *Biomaterials* **2003**, *24*, 1121.